

# Fracture mechanics of shape memory alloys: review and perspectives

T. Baxevanis · D. C. Lagoudas

Received: 24 December 2014 / Accepted: 31 January 2015 / Published online: 17 February 2015  
© Springer Science+Business Media Dordrecht 2015

**Abstract** Shape memory alloys (SMAs) are inter-metallic alloys displaying recoverable strains that can be an order of magnitude greater than in traditional alloys due to their capacity to undergo a thermal and/or stress-induced martensitic phase transformation. Since their discovery, the SMA industry has been dominated by products for biomedical applications with geometrically small feature sizes, especially endovascular stents. For such products the technological importance of fracture mechanics is limited, with the emphasis being placed on preventing crack nucleation rather than controlling crack growth. However, the successful integration of SMAs into commercial actuation, energy absorption, and vibration damping applications requires understanding and practice of fracture mechanics concepts in SMAs. The fracture response of SMAs is rather complex owing to the reversibility of phase transformation, detwinning and reorientation

of martensitic variants, the possibility of dislocation and transformation-induced plasticity, and the strong thermomechanical coupling. Large-scale phase transformation under actuation loading paths, i.e., combined thermo-mechanical loading, and the associated configuration dependence complicate the phenomenon even further and question the applicability of single parameter fracture mechanics theories. Here, the existing knowledge base on the fracture mechanics of SMAs under mechanical loading is reviewed and recent developments in actuation-induced SMA fracture are presented, in terms of the micro-mechanisms of fracture, near-tip fracture environments, fracture criteria, and fracture toughness properties.

**Keywords** Shape memory alloys · Fracture mechanics · Phase transformation · Finite element analysis

## 1 Introduction

The unique and closely related properties of *shape memory* and *pseudoelasticity* (also referred to as super-elasticity) in SMAs result from a reversible, diffusionless solid-to-solid transformation from austenite to martensite and *vice versa* under applied mechanical load and/or temperature variations (Otsuka and Wayman 1999; Lagoudas 2008). The parent austenite phase transforms to the martensite phase upon cooling, through the martensitic-start ( $M_s$ )—martensitic-finish ( $M_f$ ) temperature interval, which is depen-

---

**Electronic supplementary material** The online version of this article (doi:10.1007/s10704-015-9999-z) contains supplementary material, which is available to authorized users.

---

T. Baxevanis (✉)  
Department of Aerospace Engineering, Texas A&M  
University, College Station, TX 77843, USA  
e-mail: theocharis@tamu.edu

D. C. Lagoudas  
Department of Aerospace Engineering & Department of  
Materials Science and Engineering, Texas A&M  
University, College Station, TX 77843, USA

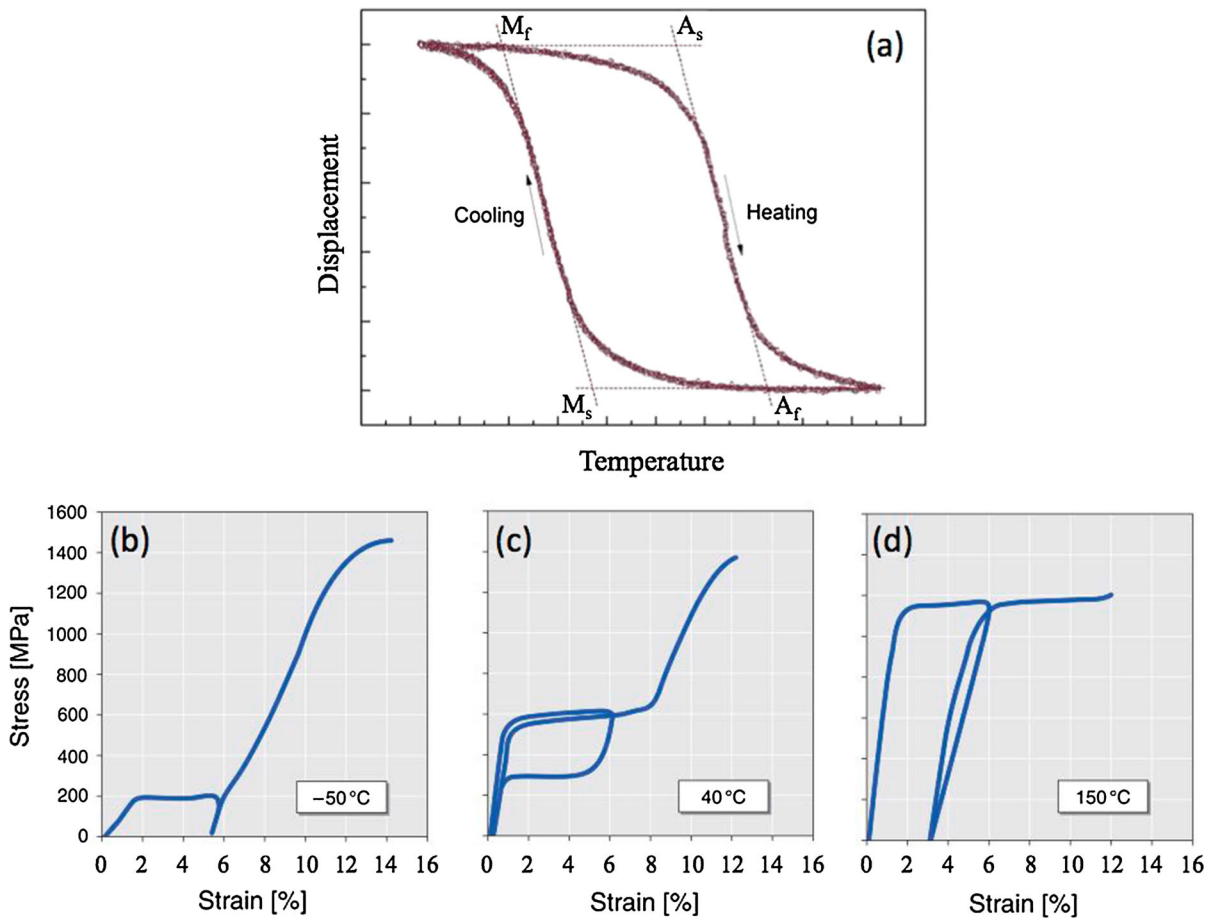


**Fig. 1** **a** Schematic of displacement-temperature response under constant load. Isothermal tensile stress-strain response of Nitinol at different test temperatures: **b** at  $-50^{\circ}\text{C} < M_f$ , the structure is martensite and detwinning takes place under sufficient applied loading. Upon continued loading, the material deforms plasti-

cally via slip; **c** at  $40^{\circ}\text{C} > A_f$ , the structure is austenite and its behavior is pseudoelastic. For stress levels beyond the initial loading plateau, martensite behaves similarly to a conventional alloy; **d** at  $150^{\circ}\text{C} > M_d$ , austenite deforms as a conventional alloy. After Pelton et al. (2000)

dent on composition, material processing, and stress levels (Fig. 1a). In the absence of mechanical load, the variants of the low-symmetry martensite phase usually arrange themselves in a self-accommodating manner through twinning, resulting in no observable macroscopic shape change. Contrary, under sufficient mechanical load, only favorably oriented martensitic variants form leading to large macroscopic inelastic strains. During heating, martensite reverse transforms back to austenite in a temperature interval defined by the austenitic-start ( $A_s$ ) and austenitic-finish ( $A_f$ ) temperatures, and the inelastic strains are recovered (shape memory effect). At intermediate temperatures between  $M_s$  and  $M_f$  or  $A_s$  and  $A_f$ , there is a two phase mixture of austenite and martensite. If a mechanical load

is applied to the material in the twinned martensite phase, detwinning is possible by reorientation of a certain number of variants (Fig. 1b). The high inelastic strains associated to detwinning are not recovered upon removal of the load, while plastic deformation may occur upon continued loading. Pseudoelasticity involves stress-induced transformation from austenite to detwinned martensite, followed by strain recovery (and concomitant phase transformation back to the parent austenite phase) upon unloading (Fig. 1c). Beyond the initial loading plateau corresponding to martensitic transformation, the material's deformation response is similar to that of a conventional alloy. For nominal temperatures above  $M_d$ , the austenite phase is stable and the resulting stress-strain curve is that of a conven-

tional alloy, with plastic deformation occurring when the stress reaches the yield stress of austenite (Fig. 1d).

A vast literature has been established over the years that addresses the phenomenology and modeling approaches of SMA behavior [see the review articles of Patoor et al. (2006), Lagoudas et al. (2006) and the book edited by Lagoudas (2008)]. There has also been significant research into the mechanical fatigue behavior of conventional SMAs [see the review of Robertson et al. (2012)], stemming mainly from their suitability for medical applications (Miyazaki 1990; Duerig et al. 1999; Stoeckel et al. 2004; Petrini and Migliavacca 2011). Limited studies, however, both experimental and analytical, are devoted to the fracture mechanics and properties of SMAs. One of the reasons for the limited interest in the fracture behavior of SMAs is that commercial applications are dominated by products with geometrically small feature sizes subject to low service loads for which fracture mechanics are generally irrelevant. Fracture mechanics is most appropriate when the geometric size of the product is large enough to sustain stable crack growth and retain functionality despite the presence of a growing crack. One example of a product that meets such a description is high power output solid state SMA actuators. Their forthcoming commercial use in non-biomedical applications such as aeronautics, energy conversion and storage, and automotive is expected to increase drastically the technological importance of fracture in SMAs. SMA actuators take advantage of the shape memory effect to provide high actuation energy density, can perform the functions of several materials and parts simultaneously, thus simplifying the device design, have fewer parts to break or wear down, and are therefore attractive as an alternative to electromagnetic actuators (Hartl and Lagoudas 2007; Sreekumar et al. 2007; Nespoli et al. 2010) (Fig. 2).

The data available in the literature is entirely devoted to fracture of SMAs under quasi-static mechanical loading. Fracture of SMAs under these conditions bears similarities with fracture of other dissipative systems, such as conventional elastic-plastic materials. For example, fracture toughening response is observed associated with crack advance that should be attributed to the hysteretic stress–strain excursions experienced by material elements close to the crack tip resulting in dissipated energy that must be supplied by the external loading in order to maintain crack growth (Robertson and Ritchie 2007, 2008; Yi and Gao 2000; Freed

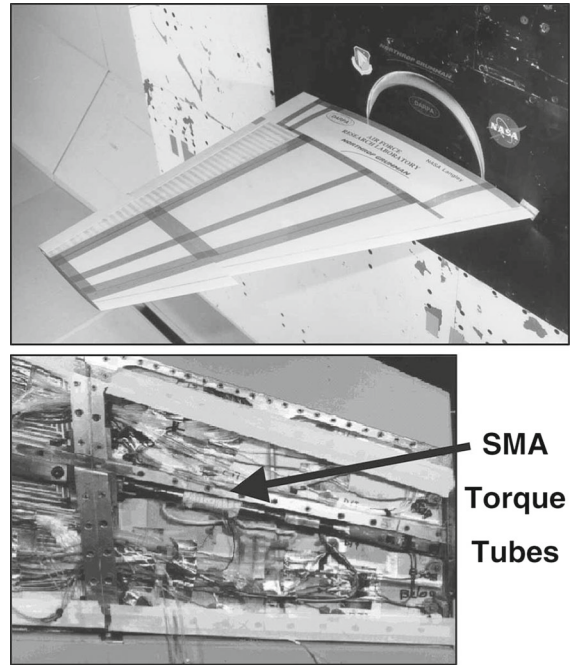
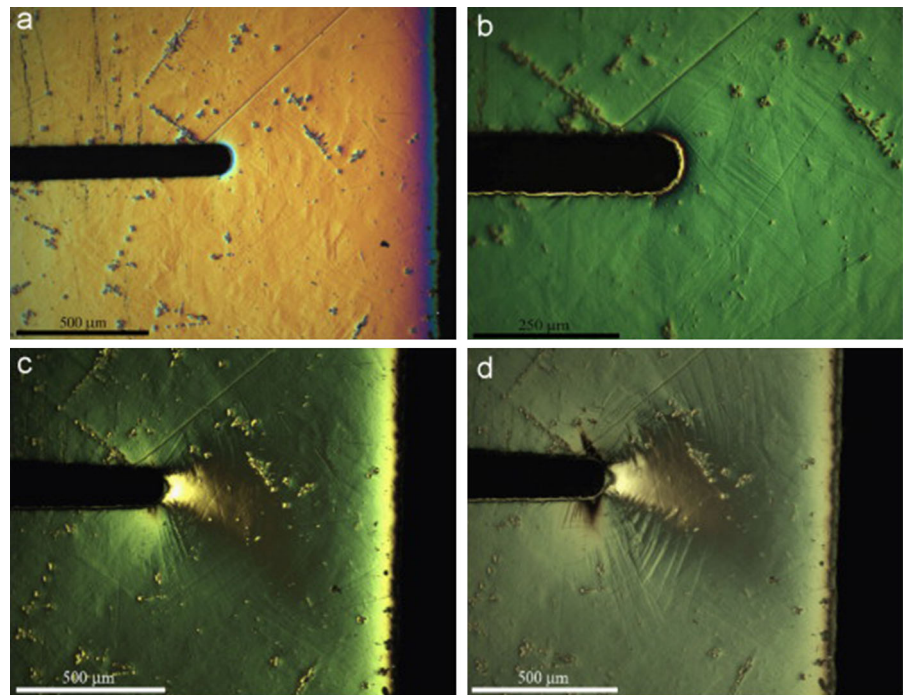


**Fig. 2** Total and cut-away view of the SMA torque tube as installed in the model wing during phase I of the SMART wing project. After Hartl and Lagoudas (2007)

and Banks-Sills 2007; Baxevanis et al. 2014b). Fracture under actuation loading paths, i.e., under combined thermo-mechanical loading, to the best of the authors' knowledge, has not yet been addressed. As recently observed, notched  $\text{Ni}_{60}\text{Ti}_{40}$  (wt%) SMA specimens may fail by formation of an unstable crack during cooling, under a low, compared to the isothermal strength at the beginning of cooling, constant applied tensile load.<sup>1</sup> This behavior, which from an energetic point of view may seem in disagreement with the general view of dissipative processes resulting in an enhancement of fracture toughness, is characteristic of SMAs and should be attributed to global phase transformation from austenite to martensite interacting with the stress field near the notches (Baxevanis et al. 2015). In most conventional elastic-plastic metals, cooling under a constant load does not considerably affect the existing plastic zone close to the crack tip and thermal contraction results in crack shielding rather than anti-shielding. Application of classical elastic-plastic fracture mechanics as a quantitative tool for actuation-induced crack growth in SMAs is rather challenging. Global transformation

<sup>1</sup> On going work that is presented in Sect. 3.1.

**Fig. 3** Progression of transformation and crack propagation in single crystal  $\text{Ni}_{50.8}\text{Ti}_{49.2}$  (at%) with the crystallographic direction  $[111]$  aligned with the loading axis. **a** Transformation prior to loading. **b** Growth of “micro-transformation” of martensite ahead of the notch tip. **c** Growth of transformation zone, with martensite plates both ahead and to the side of the notch. **d** Immediately prior to fracture, a significant amount of out of plane deformation has occurred ahead of the notch, as indicated by the bright region. After [Creuziger et al. \(2008\)](#)



during thermomechanical loading through the martensitic transformation temperatures and associated configuration dependence question the applicability of single parameter fracture mechanics theories.

This paper reviews experimental findings and modeling efforts on SMA fracture response under mechanical loading (Sect. 2) and discusses recent developments in actuation-induced SMA fracture (Sect. 3). The paper concludes with a discussion of future experimental and modeling research priorities that may have the greatest impact on understanding the fracture properties and practice fracture mechanics concepts in SMAs (Sect. 4).

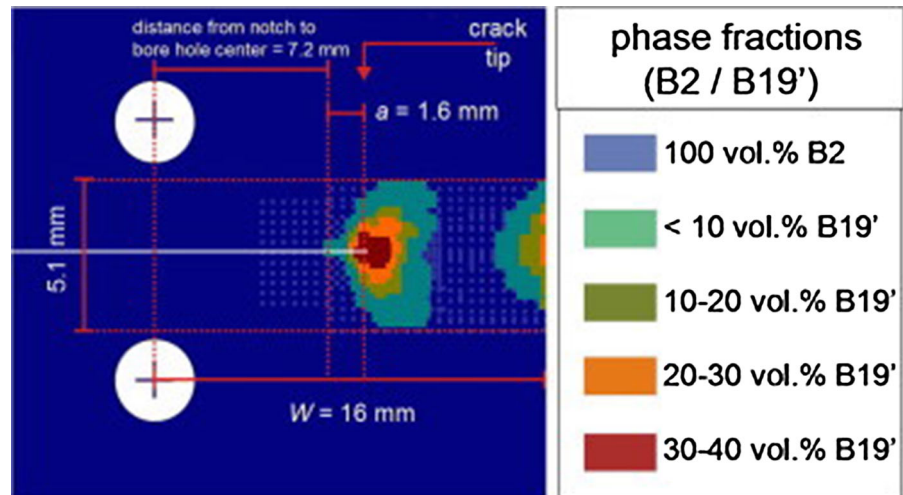
## 2 Fracture of SMAs under mechanical loading

In this section the knowledge acquired on the fracture response of SMAs under mechanical loading is reviewed. The fracture response of SMAs is more complex than that of common structural metals due to their unique thermomechanical behavior, although some similarities would be evident in the discussion. Both the experimental findings and the developments in modeling are addressed.

### 2.1 Experimental studies of fracture processes

Most of the existing experimental studies on the fracture response of SMAs have been devoted to NiTi alloys. At constant ambient temperatures, stress-induced phase transformation near the crack tip in pseudoelastic polycrystalline NiTi was reported by [Robertson et al. \(2007b\)](#) and [Gollerthan et al. \(2009b\)](#), by [Creuziger et al. \(2008\)](#) in single crystalline NiTi (Fig. 3), and by [Vasko et al. \(2002\)](#) and [Loughran et al. \(2003\)](#) in single crystalline Cu-based SMAs. [Robertson et al. \(2007b\)](#) suggested that the formation of stress-induced martensite could be suppressed under plane strain conditions due to the high hydrostatic tensile stress levels in front of the cracks. However, [Gollerthan et al. \(2009b\)](#) and [Young et al. \(2013\)](#) using in situ synchrotron X-ray diffraction experiments provided definitive crystallographic evidence of fully reversible stress induced martensite ahead of a crack in plane strain specimens (Fig. 4). In situ synchrotron X-ray diffraction measurements were also used by [Daymond et al. \(2007\)](#) to create two dimensional maps of elastic strain and texture near the crack tip in martensitic NiTi compact tension (CT) specimens. High tensile strains were measured within and beyond the detwinning zone

**Fig. 4** Phase fractions of the austenite B2 and martensite B19' structures for the two transformation zones—one close to the crack tip (tensile in nature) and the other one at the far end of the specimen (compressive in nature)—in a pseudoelastic polycrystalline Ni<sub>50.7</sub>Ti<sub>49.3</sub> (at%) SMA CT specimen obtained by in situ synchrotron measurements at high stress intensity. After Gollerthan et al. (2009b)



observed in the vicinity of the crack tip, with this strain field becoming compressive upon unloading.

Fracture toughness values of NiTi SMAs have been reported in just a few papers (Holtz et al. 1999; Gollerthan et al. 2009b; Vaidyanathan et al. 2000; Robertson et al. 2007a). As discussed in the review paper of Robertson et al. (2012), most of the published data appears to be determined from test specimens of thickness not large enough compared with the estimate of the plastic zone size in conventional elastic-plastic materials,  $1/(3\pi) \cdot (K_{Ic}/\sigma_y)^2$  (Irwin 1968), i.e., their thickness did not exceed  $2.5(K_{Ic}/\sigma_y)^2$  where  $K_{Ic}$  is the calculated critical stress intensity factor and  $\sigma_y$  the yield stress of the material. Therefore these tests do not comply with the small yielding condition which is a prerequisite for measuring the critical stress intensity factor in conventional elastic-plastic materials. Vaidyanathan et al. (2000), Gollerthan et al. (2009b), and Robertson et al. (2007a) all measured, based on the premise of linear elastic fracture mechanics (LEFM) by using test specimens of sufficient size to the previous constraint, nearly identical  $K_{Ic}$ -values of  $\sim 30 \text{ MPa}\cdot\text{m}^{1/2}$  for pseudoelastic Nitinol (Fig. 5). Nonetheless, these results are as well questionable, since ASTM standards should be interpreted as to require the zone of non-linear deformation close to the crack tip, regardless of the mechanism, to be smaller than a fraction of all the characteristic dimensions of the crack configuration. With respect to SMAs, this restriction leads to a requirement on the size of the stress-induced transformation/detwinning zone, not on the plastic zone size, being small enough for LEFM to

be valid. Although the expression  $1/(3\pi) \cdot (K_{Ic}/\sigma_y)^2$  overestimates, by an order of magnitude, the size of the yielding zone in SMAs (Baxevanis et al. 2012), it underestimates considerably the size of the transformation/detwinning zone, which can be approximated as  $1/(3\pi) \cdot (K_{Ic}/\sigma_{cr})^2$ . In this expression,  $\sigma_{cr}$  denotes either the stress level required for initiation of phase transformation or the stress level required for detwinning of twinned martensite depending on whether the material is in the austenitic or twinned martensitic state at zero load, respectively, and the ambient temperature is below  $M_d$ . For higher temperatures,  $\sigma_{cr}$  should be understood as the yield stress of austenite. For such a requirement to be satisfied, the SMA specimens may be prohibitively large depending on the ambient temperature. An alternative is to measure the fracture toughness using the  $J$ -integral as a fracture criterion, for which the requirements on specimen sizes are much less strict than those for a valid  $K_{Ic}$ -value. Preliminary data from experiments complying with ASTM Standard E1820 (2013) requirements for the size of the transformation/detwinning zone<sup>2</sup> show that the critical  $J$ -value for crack growth varies by less than 13% in an ambient temperature range that includes all the phase transition temperatures (Fig. 6). As the fracture toughness is influenced mostly by the microstructure in the immediate vicinity of the crack tip, it is perhaps not surprising that reliable fracture toughness measurements may yield nominally constant values at different ambi-

<sup>2</sup> Private communication with Dr. Karaman's group at Texas A&M University.

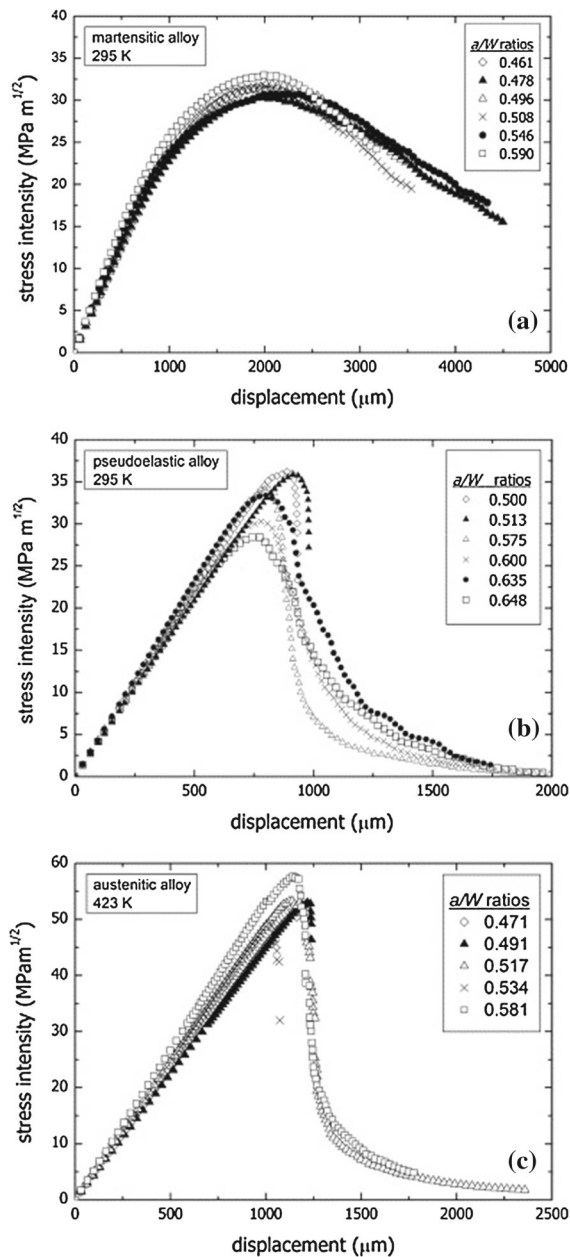


**Fig. 5** Stress intensity ( $K^*$ ) versus displacement curves of **a** martensitic  $\text{Ni}_{50.3}\text{Ti}_{49.7}$  (at%) SMA at 295 K; **b** pseudoelastic  $\text{Ni}_{50.7}\text{Ti}_{49.3}$  (at%) SMA at 295 K, and **c** austenitic  $\text{Ni}_{50.7}\text{Ti}_{49.3}$  (at%) SMA at 423 K (temperature above  $M_d$ ) with varying  $a/W$  ratios. The \* was used by the authors to indicate that the severe constraints imposed by the LEFM are not fully met in their experiments.  $a$  is the crack length and  $W$  the thickness of their specimen.  $\text{Ni}_{50.7}\text{Ti}_{49.3}$  (at%) was heat treated at 500 °C for 6 min. After Gollerthan et al. (2009b)

ent temperatures as long as a martensitic zone exists close to the crack tip.

In terms of micro-mechanisms of fracture, cleavage fracture and ductile tearing were found to act in conjunction in precipitated single crystalline and polycrystalline NiTi SMAs, with the relative dominance of one over the other depending on the local precipitate size and concentration (Gall et al. 2001) (Fig. 7). Distinct cleavage fracture and river markings consistent with markings from traditional brittle intermetallic alloys were reported in material systems containing semi-coherent  $\text{Ti}_3\text{Ni}_4$  precipitates (50–150 nm), while for incoherent precipitates (400 nm) the overall fracture is dominated by ductile tearing, and the cleavage markings become diffuse. Gollerthan et al. (2009b) observed that the crack tips stay sharp during crack growth in NiTi and do not exhibit the typical features associated with crack tip blunting in conventional ductile materials (Fig. 8). Crack tip blunting is associated with dislocation processes, and the absence of blunting in NiTi may well reflect the fact that dislocation activity at the crack tip plays a much smaller role. Moreover, all martensitic features in front of the crack tip were found to disappear after unloading. This observation excludes the formation of stabilized martensite, which cannot reverse transform, because it is hindered by the presence of dislocations. Further work is required to clarify the effect of dislocations in NiTi when cracks grow in pseudoelastic SMAs.

The crack-tip stress-induced phase transformation/detwinning is primarily responsible for the phenomenon of stable crack growth (transformation toughening) observed in single crystalline (Loughran et al. 2003; Creuziger et al. 2008) and polycrystalline SMAs. Robertson and Ritchie (2007, 2008) were the only ones who presented evidence of stable crack growth in NiTi in the form of rising R-curves in polycrystalline SMAs (Fig. 9). Gollerthan et al. (2009a) provided direct physical evidence for reverse transformation of stress-induced martensite expected to occur due to unloading in the material regions left behind the advancing crack tip. IR thermography was used to observe thermal changes on the material's surface which can indicate heat flows associated with martensitic forward and reverse transformations (Fig. 10).

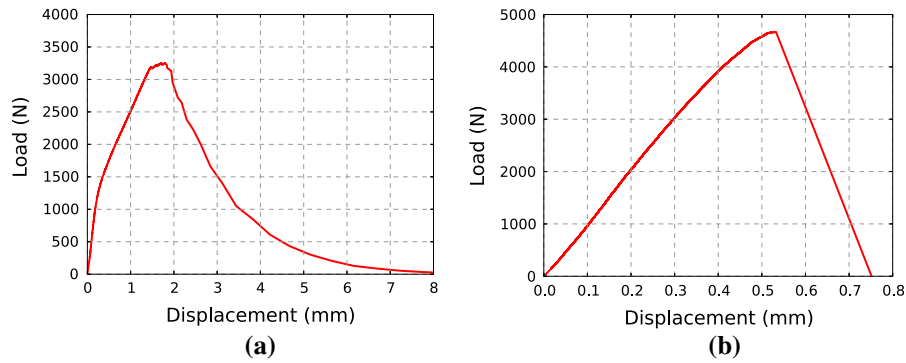
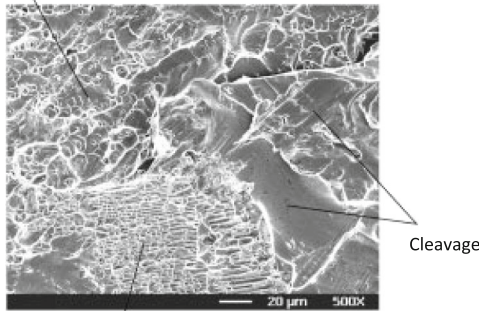


**Fig. 6** Load versus displacement from experiments conducted on CT specimens of Ni<sub>50.7</sub>Ti<sub>49.3</sub> (at%) heat treated at 300 °C for 100 h. **a** Tested at  $M_s = -2$  °C (martensitic state). The obtained

critical  $J$ -value for crack growth obtained is 36.05 KJ/m<sup>3</sup>. **b** Tested at  $A_s + 10 = 70$  °C (austenitic state). The obtained critical  $J$ -value for crack growth obtained is 32.23 KJ/m<sup>3</sup>

Void nucleation, growth, and coalescence from Ti<sub>3</sub>Ni<sub>4</sub> precipitates



Void nucleation, growth, and coalescence from fractured Ti-C inclusions

**Fig. 7** Representative SEM image from a crystal aged 1.5 h @ 823 K and loaded along the [148] crystallographic direction, demonstrating the three different fracture mechanisms observed in the precipitated Ni<sub>50.7</sub>Ti<sub>49.3</sub> (at%). After Gall et al. (2001)

## 2.2 Analytical and numerical modeling of fracture response

### 2.2.1 Static cracks

As discussed in the previous section, the size of the stress-induced transformation zone as a function of the loading conditions is important in experimental investigations of the fracture toughness of SMAs. Xiong and Liu (2007), Maletta and Furgieue (2010, 2011), Maletta and Young (2011), Maletta (2012) and Maletta et al. (2013) adopted analytical approaches in determining the size of the stress-induced phase transformation

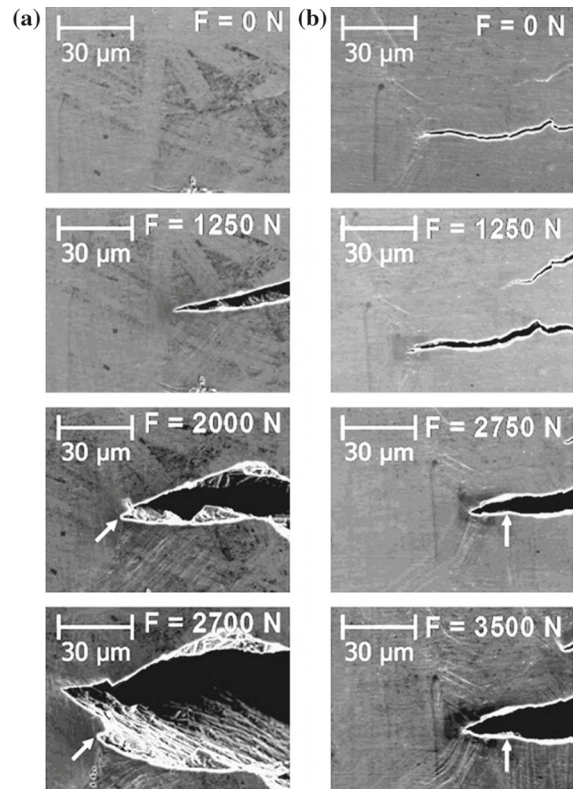


**Fig. 8** Scanning electron micrographs of **a** martensitic and **b** pseudoelastic NiTi SMAs at applied loads of 0, 1250, 2000 and 2700 N and 0, 1250, 2750 and 3500 N, respectively, during an in situ fracture experiment. After Gollerthan et al. (2009b)

zone under mode I, in the realm of Irwin's correction of LEFM, that accounts for the stress redistribution due to transformation around the crack tip on the basis that the stress resultant along the plane of the crack should be

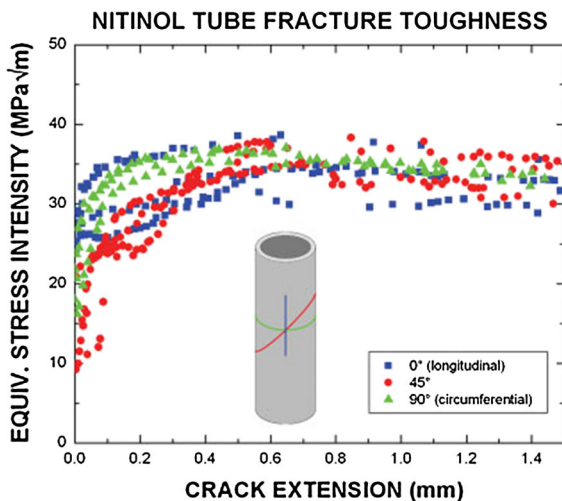


**Fig. 9** Fracture toughness in terms of crack-resistance (R-curve) data for thin-walled pseudoelastic Nitinol tube tested in 37 °C air. Crack-initiation toughness values were significantly lower than those at steady-state, and depended strongly on crack-propagation direction within the tube. After Robertson and Ritchie (2008)

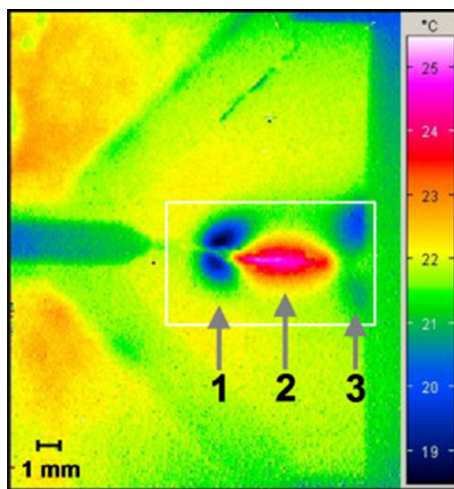


**Fig. 10** Thermographic image obtained during in situ dynamic loading of a pseudoelastic Ni<sub>50.7</sub>Ti<sub>49.3</sub> (at%) SMA CT specimen providing direct physical evidence for reverse transformation of stress-induced martensite in the wake of the advancing crack tip. The three arrows indicate the crack tip position prior to crack propagation (arrow 1), the actual crack position (arrow 2), and a region ahead of the crack tip (arrow 3). After Gollerthan et al. (2009a)

equal to the stress resultant of linear elasticity. In deriving their model, Maletta and Furguele (2010, 2011), Maletta and Young (2011), Maletta (2012) and Maletta et al. (2013) excluded the possibility of plastic yielding,

while Xiong and Liu (2007) did include plastic yielding in their model but assumed a linear stress distribution in the region of elastically-deformed, fully-transformed material close to the crack tip; an assumption which is not consistent with numerical results (Baxevanis et al. 2012). Lexcellent and Thiebaud (2008), Lexcellent et al. (2011a, b) and Birman (1998) evaluated the size of the transformation zone without taking into account the stress redistribution caused by transformation. In all the above investigations, simple closed form expressions were derived that can be potentially used for the purpose of determining experimentally the fracture toughness of SMAs. Comparison against experiments whenever offered in the above investigations revealed that many of these closed form expressions if not all can offer reliable estimates of the transformation zone size close to the crack tip (Fig. 11). For relatively small transformation sizes with respect to crack length, even the estimate  $1/(3\pi) \cdot (K_{Ic}/\sigma_{cr})^2$ , introduced in the previous section, which treats transformation as being similar to perfect plasticity, is acceptable. Baxevanis and Lagoudas (2012) introduced a model that incorporates transformation and plasticity into the model formulation proposed by Dugdale (1960) for conventional elastic-plastic materials under plane stress conditions. Utilizing this model the sizes of the various zones formed in front of the crack tip were evaluated and closed form expressions of the  $J$ -integral were obtained depending on the value of the remote stress levels. The size of the plastic and transformed regions near the crack tip for mode III loading of SMAs were approximated by Desindes and Daly (2010).

Finite element analysis on the stress-induced martensitic transformation near the stationary crack tip or notch of CT SMA specimens has also been performed in the literature (Fig. 12). In Wang et al. (2005) it was shown, using a constitutive model that neglects plastic yielding, that the extent of the transformation zone is load path dependent due to the hysteretic stress-strain behavior of SMAs and that the formation of martensite results in a redistribution process where the stresses near the crack tip relax. The numerical analysis of Wang (2007a, b) showed that martensite transformation increases the required load to produce plastic deformation and decrease the maximum normal stress near the notch tip. Their calculations were based on an elastic-plastic material model calibrated by an experimental monotonic tensile stress-strain relation to account for both transformation and plasticity.



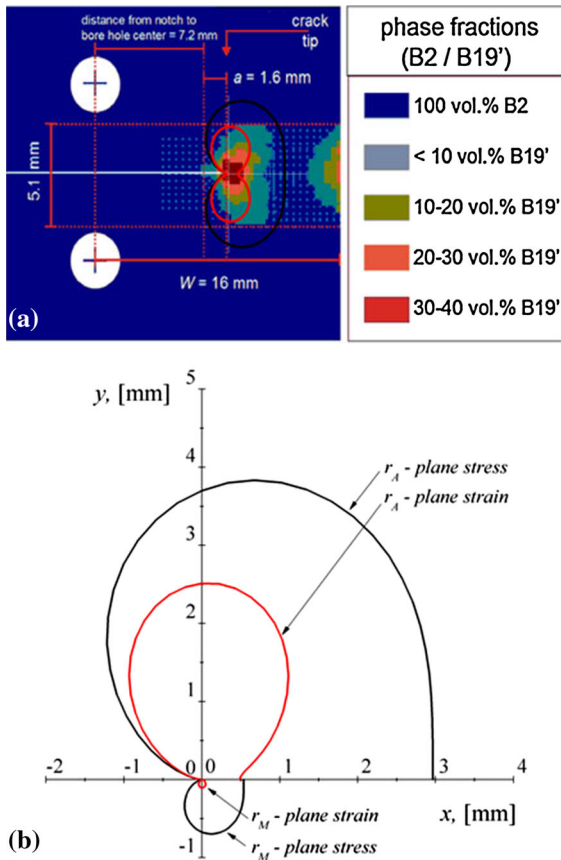


**Fig. 11** Contours of the transformation region for a miniature CT specimen with a crack length-to-width ratio  $a/W = 0.55$  under a constant load  $P = 2860$  N: **a** comparison of the austenitic radius  $r_A$  between numerical predictions and experimental observations by synchrotron x-ray micro-diffraction (Gollerthan et al. 2009b); **b** austenitic radius,  $r_A$ , and martensitic radius,  $r_M$ , under plane stress and plane strain conditions. After Maletta and Young (2011)

Baxevanis et al. (2012) arrived at a similar conclusion for SMAs obeying power-law hardening flow theory for the evolution equations of the plastic strains showing that stress redistribution due to stress-induced martensitic transformation results in plastic zone sizes at the vicinity of the crack tip an order of magnitude smaller than the size expected in conventional elastic-plastic materials (Fig. 13). Moreover, it was shown that the singularity form and the angular variation of the strain and stress fields close to the crack tip can be approximated by the asymptotic solutions found by Hutchinson (1968) and Rice and Rosengren (1968) for power-law hardening deformation plasticity theory. The intensity of the singularity, however, does not correspond to that

of the asymptotic solutions. Furthermore, the validity of the  $J$ -integral as a fracture criterion for pseudoelastic SMAs was investigated. Although the  $J$ -integral was found to be path-dependent for mode I loading,<sup>3</sup> from an engineering point of view, the assumption of a fracture toughness criterion for SMAs based on the path-independence of the  $J$ -integral, a common practice in conventional elastic-plastic materials, could be justified in the sense that the difference between the crack-tip and far-field  $J$ -values in SMAs is smaller than the corresponding difference in elastic-plastic materials (Fig. 14).

### 2.2.2 Crack growth

There have been few theoretical and numerical investigations on the toughening effect of stress-induced phase transformation associated with quasi-static crack advance in pseudoelastic SMAs.<sup>4</sup> Yi and Gao (2000) and Yi et al. (2001) studied the fracture toughness of SMAs under mode I and mixed mode conditions. The transformation volume strain was assumed negligible compared to the resulting shear strain, and was thus ignored. Their analyses followed closely that of McMeeking and Evans (1982) and Budniansky et al. (1983) using LEFM theory together with the Eshelby equivalent inclusion method to obtain resistance  $R$ -curves. Yan and Mai (2006) studied the combined effect of stress-biased transformation shear strain and volumetric strain (0.39% volume contraction) and an overall enhancement of the fracture toughness was shown in accordance with the aforementioned investigations. All these works assume that once a level of stress is

<sup>3</sup> Rice (1968, 1967) demonstrated path-independence of the  $J$ -integral for flow theory plasticity near stationary crack tips loaded in mode III in elastic-power-law hardening materials under the small-scale yielding assumption. There is no such proof for in-plane loading modes. Actually, finite element calculations have shown that  $J$  is path-dependent near stationary crack tips for loadings with a mode I component in elastic-power-law hardening materials obeying flow plasticity theory (Carka and Landis 2011).

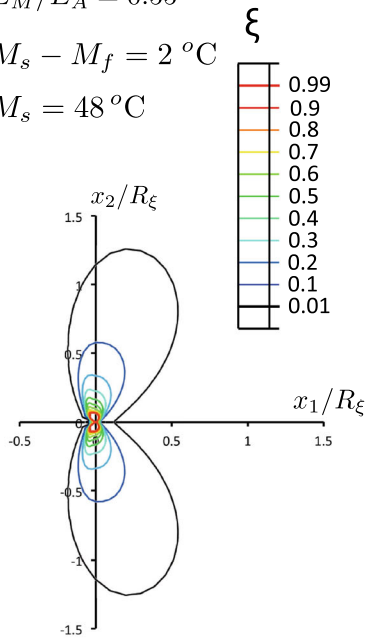
<sup>4</sup> A video of simulated quasi-static stable crack growth in an SMA material and the resulted toughness enhancement measured in the terms of the ratio of the loading parameter,  $K_I$ , to its critical value for initiation of crack growth,  $K_{Ic}$  under the small-scale transformation assumption can be found here (Supplementary material 1) (see Baxevanis et al. (2013) for the details of the simulation).  $\delta a$  denotes increments of the crack length  $a$  and  $R_\xi$  the approximated size of the transformation zone at initiation of crack growth.

$$H = 0.06$$

$$E_M/E_A = 0.55$$

$$M_s - M_f = 2 \text{ }^\circ\text{C}$$

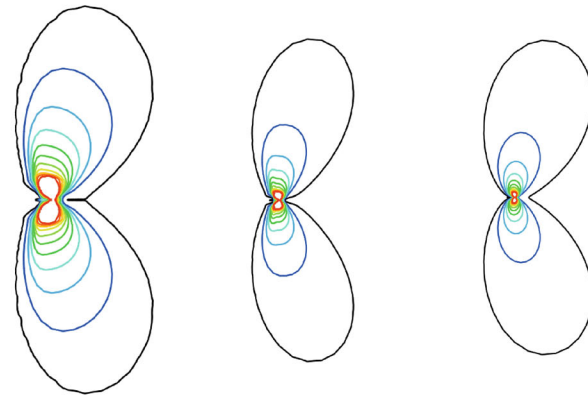
$$M_s = 48 \text{ }^\circ\text{C}$$



$$H = 0.02$$

$$E_M/E_A = 1$$

$$M_s - M_f = 30 \text{ }^\circ\text{C}$$



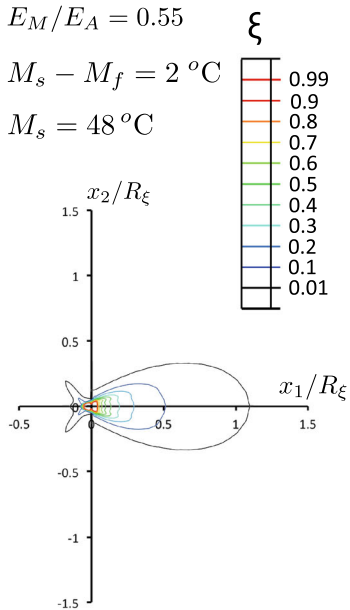
(a)

$$H = 0.06$$

$$E_M/E_A = 0.55$$

$$M_s - M_f = 2 \text{ }^\circ\text{C}$$

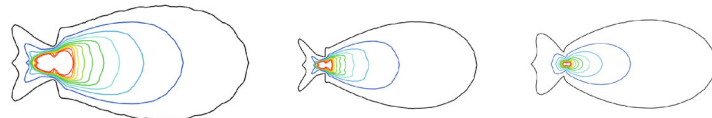
$$M_s = 48 \text{ }^\circ\text{C}$$



$$H = 0.02$$

$$E_M/E_A = 1$$

$$M_s - M_f = 30 \text{ }^\circ\text{C}$$



(b)

**Fig. 12** Transformation zone boundary and contour plot of the martensite volume fraction. The first contour plot in each sub-figure is obtained for the parameter values indicated on top of them. The value of the parameter changed in obtaining each of

the other contour plots is also indicated above them.  $H$  is the maximum transformation strain,  $E_M$  and  $E_A$  are the Young's moduli of martensite and austenite, respectively. After [Baxevanis et al. \(2012\)](#)

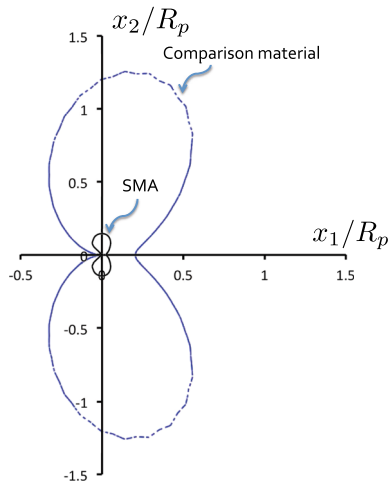


**Fig. 13** The inner curve represent the plastic zone boundary in an SMA material under mode I loading and the outer one the plastic zone boundary of the SMA without accounting for phase transformation, i.e., considering the SMA as an elastic-plastic material. The spatial variables are normalized with respect to  $R_p = 1/(3\pi) \cdot (K_I/\sigma_Y^M)^2$ , where  $K_I$  is the far-field stress intensity factor in the small-scale transformation conditions adopted in the calculations and  $\sigma_Y^M$  is the yield stress of martensite. After Baxevanis et al. (2012)

achieved at a material point, a finite pre-determined level of transformation strain is instantaneously accumulated, i.e., transformation is all or none, and there is no partial transformation allowed. This is an approximation to the actual SMA constitutive behavior which results in a non-uniform distribution of transformation strains and a zone of partial transformation close to the crack tip even when transformation takes place at a constant stress level.

Stam and van der Giessen (1995) examined the effect of reverse phase transformation on the crack growth resistance in the pseudoelastic regime in a finite element framework of crack propagation under small-scale transformation conditions. They found that reverse transformation can significantly reduce the resistance increase. Freed and Banks-Sills (2007) arrived at a similar conclusion in their study of the growth resistance in an SMA under plane strain, mode I conditions by means of a cohesive zone model. The analysis of Stam and van der Giessen (1995) was based on the aforementioned assumption that transformation is all or none while the constitutive model employed in the calculations of Freed and Banks-Sills (2007) is valid only for proportional loading. It may give non-zero transformation strain for a null martensite volume

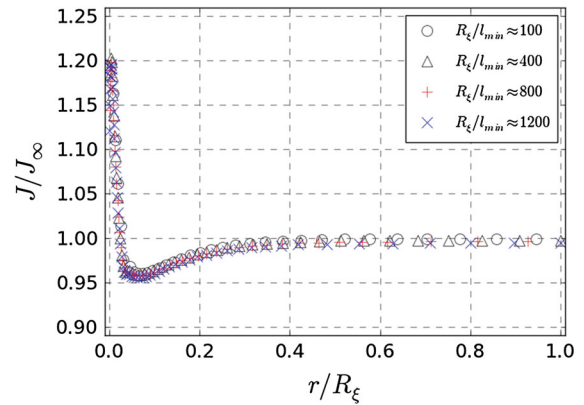


**Fig. 14**  $J$ -integral values versus the radius of the circular integration contour for mode I loading. The markers correspond to different load levels from the same simulation illustrating the self-similarity of the solution. These different load levels are represented by the size of the corresponding transformation zones  $R_\xi$  which are 100, 400, 800 and 1200 times the radial dimension of the first ring of elements surrounding the crack tip,  $l_{min}$ , indicating the amount of refinement in each of these load levels.  $J_\infty$  is the far-field  $J$ -value. After Baxevanis et al. (2012)

fraction upon reverse phase transformation under non-proportional loading such as that experienced by material elements near the passing crack tip. The analysis of quasi-static steady crack growth of Baxevanis et al. (2014b) is free from those deficiencies. According to their calculations, reverse phase transformation increases the levels of toughness enhancement due to the associated dissipation of energy, as seen in Fig. 15. In these calculations, the required stress level for initiation of forward transformation was kept constant by fixing the ambient temperature  $T$  and the martensitic-start and -finish temperatures, while the austenitic-start and -finish temperatures were shifted closer to  $M_s$  to increase the tendency of the material to reverse transform back to austenite in the wake of the growing crack. For a specific material system, however, higher ambient temperatures result in higher stress levels required for initiation of forward transformation, which in turn impedes transformation reducing the levels of toughness enhancement, although the material's tendency to reverse transform in the wake of the advancing crack is stronger. That is essentially what Freed and Banks-Sills (2007) reported when they argued that reverse transformation can significantly reduce the resistance increase.

The dependence of transformation toughening on the transformation strain, slopes of the stress-strain curve during transformation, extent of reverse phase

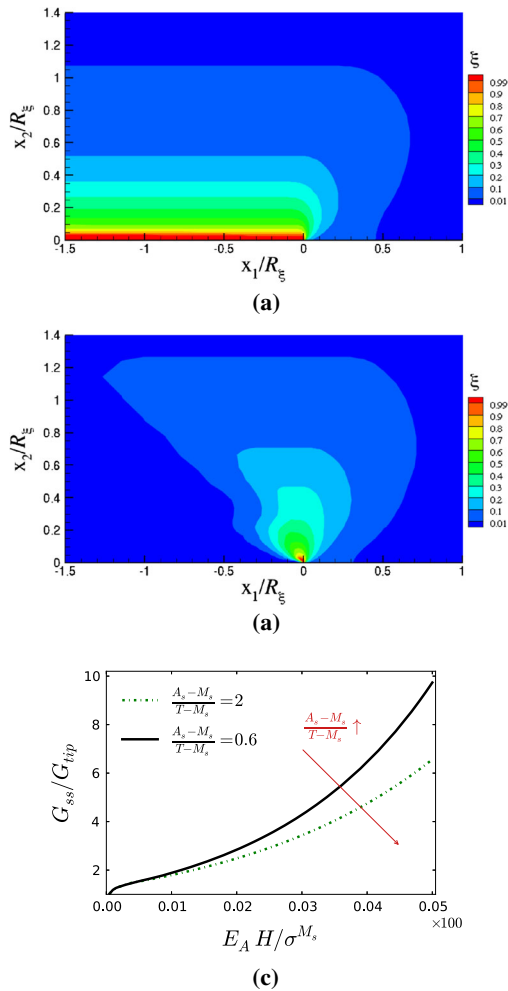


**Fig. 15** Martensite volume fraction,  $\xi$ , close to the steadily advancing crack tip and fracture toughness enhancement for two values of the non-dimensional parameters  $(A_s - M_s)/(T - M_s)$ , where  $T$  denotes the ambient temperature. The values of the other non-dimensional parameters used in the calculations are given in Baxevanis et al. (2014b). Decreasing ratios  $(A_s - M_s)/(T - M_s)$  correspond to a stronger tendency of the material to reverse transform in the wake of the growing crack and therefore to larger material volumes that reverse transform back to austenite resulting in higher levels of toughness enhancement. Due to symmetry conditions the results are displayed on the upper half plane. The crack tip is located at  $(x_1/R_\xi, x_2/R_\xi) \equiv (0, 0)$  where  $R_\xi$  approximates the height of the transformation zone. **a** Martensite volume fraction,  $\xi$ , for  $\frac{A_s - M_s}{T - M_s} = 2$ . **b** Martensite volume fraction,  $\xi$ , for  $\frac{A_s - M_s}{T - M_s} = 0.6$ . **c** The toughness enhancement,  $G_{ss}/G_{tip}$ , as a function of the relative transformation strain,  $E_A H / \sigma^{M_s}$ , for  $\frac{A_s - M_s}{T - M_s} = 2$  and  $\frac{A_s - M_s}{T - M_s} = 0.6$ .  $G_{ss}$  and  $G_{tip}$  are the far-field and crack-tip energy release rates, respectively,  $E_A$  denotes the Young's modulus of austenite,  $H$  the maximum transformation strain, and  $\sigma^{M_s}$  the required stress level for martensitic transformation at the ambient temperature

transformation occurring in the wake of the crack, mismatch of Young's moduli between the two phases, and Poisson's ratio was found relatively strong implying that the actual shape of the uniaxial isothermal stress-strain curve is important for the quantitative determination of the transformation toughening. The changes associated with deformation cycling—maximum transformation strain and hysteresis width of the loop decrease while the slopes of the stress-strain curve during transformation get steeper (Miyazaki et al. 1986; Yoon and Yeo 2008)—in the temperature range of pseudoelasticity result in reduced levels of fracture toughness enhancement and therefore degradation of the fracture properties of pseudoelastic SMAs with training is expected.

Indications based on the numerical calculations (Baxevanis et al. 2012) and experimental evidence (Gall et al. 2001; Gollerthan et al. 2009b) referenced above, suggest that the contribution of plastic dissipation on the overall fracture resistance of SMAs might be a small fraction of the respective contribution of energy dissipation due to phase transformation. In any case, as discussed in Baxevanis et al. (2013), a quantitative determination of the actual effect of plastic deformation on the fracture toughening of SMAs is a very difficult task that relies heavily on both experimentation and constitutive modeling. For example, if a cohesive model is to be used, the phenomenological traction-separation parameters should be chosen to best fit crack growth experimental data. The fitting process requires an analysis of the reference specimen used to generate the resistance curve data with iteration on all traction-separation parameters. Only then, assuming the traction-separation law is capable of representing the fracture process in a phenomenological sense and the constitutive model capable of accurately representing the SMA response in the presence of an advancing crack, can the effect of plastic dissipation on the fracture resistance be evaluated.

The isothermal assumption used in all the aforementioned studies is valid for a range of strain rates within the regime of quasi-static processes even for complex geometries and loadings (Shaw and Kyriakides 1995; Prahlad and Chopra 2003). At higher strain rates, however depending on the geometry, convective boundary conditions, and associated heat transfer, the generation or absorption of latent heat may have a strong impact on the deformation response and the stress-strain hysteresis loop area of SMAs as shown experimentally

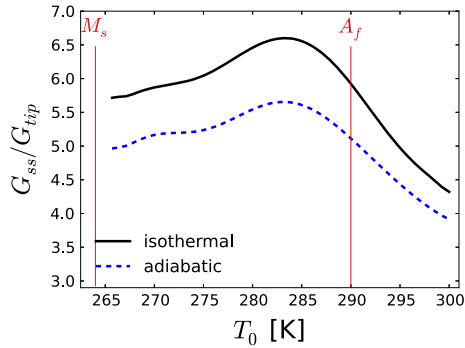


**Fig. 16** Toughness enhancement,  $G_{ss}/G_{tip}$ , as a function of ambient temperature  $T_0$  for values of the non-dimensional parameters chosen so as to conform with those of a pseudoelastic NiTi material system characterized by Machado (2007).  $G_{ss}$  and  $G_{tip}$  are the far-field and crack-tip energy release rates, respectively. After Baxevanis et al. (2014a)

(Yan et al. 2012; He et al. 2010; He and Sun 2011; Yin et al. 2013), and in turn to the fracture behavior of these materials. Given that in real applications of SMA components, the processes are usually not adiabatic, which is the case with the lowest energy dissipation during a loading-unloading process, it is expected that the actual transformation toughening would be higher than the one corresponding to the adiabatic case. For the NiTi material system investigated in Baxevanis et al. (2014a), the toughening loss due to thermomechanical coupling for mode I fracture was found less than 20% in the temperature range of interest (Fig. 16).

None of the above simulations of crack growth take into account reorientation of martensite due to unloading in the regions traversed by the advancing crack tip. Reorientation of martensite variants is expected to have an effect on the toughness enhancement due to the associated energy dissipation and stress redistribution that needs to be quantified. Hazar et al. (2015), in their analysis of *steady* state crack growth in an infinite SMA strip with fixed height, concluded that reorientation increases the levels of toughness enhancement. Their conclusion was based on a comparison between the normal to the crack plane stress component, the crack tip opening displacement, and the  $J$ -values computed for the case of reorientation included in the constitutive response and the corresponding values when reorientation was not allowed in the simulations. The comparison of the first two field-characterizing parameters for the considered cases does not quantify the effect of reorientation on the toughness enhancement as no

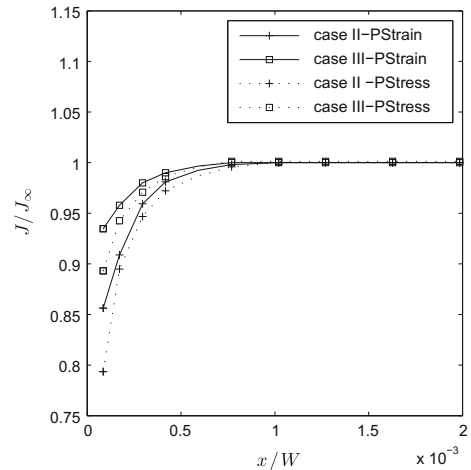


**Fig. 17**  $J$ -integrals calculated for cases II (reverse transformation with reorientation is allowed) and III (reverse transformation is allowed without martensite reorientation) under plane stress and plane strain conditions.  $J_\infty$  is the  $J$  integral far from the crack tip where the material is in the austenite phase. After Hazar et al. (2015)

comparison was made with the values of these parameters required for initiation of crack growth. As for their  $J$ -integral calculations, it is questionable whether the obtained results can be considered representative of the toughness enhancement expected due to phase transformation and reorientation. The toughness enhancement calculated is extremely small, less than 25%, i.e., an order of magnitude smaller compared with the experimental data and numerical simulations referenced above (Fig. 17).

### 3 Fracture of SMAs under thermal actuation loading paths

In this section some recent, yet unpublished, developments on the fracture mechanics of SMAs under actuation loading paths, i.e., under combined mechanical and thermal loading, are presented. The unique shape memory behavior of SMAs is shown to have a strong impact on their fracture behavior.

#### 3.1 Experimental observations

An intriguing response of SMAs was observed during thermal actuation of notched Ni<sub>60</sub>Ti<sub>40</sub> (wt%) specimens. Specimens failed during cooling, under

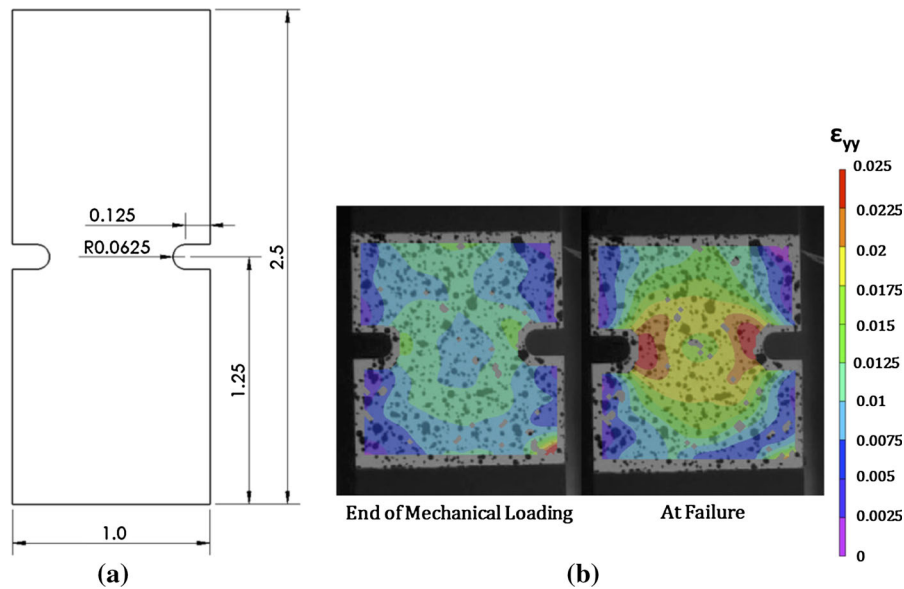


**Fig. 18** **a** Geometry of specimens. The dimensions are given in inches. The width of the specimens is 0.0591 in. **b** Strain in the direction of the tensile applied loading (vertical to the axes of the notches) at the end of the isothermal loading at 150 °C and just before the formation of an unstable crack under the same bias load

a low, compared to the isothermal strength at the beginning of cooling, constant applied tensile load. This characteristic behavior of SMAs is attributed to global thermomechanically-induced phase transformation from austenite to martensite interacting with the resulting stress field near the notches. For the U-shape notched specimens tested (Fig. 18), failure by the formation of an unstable crack during cooling was observed for bias load levels as low as 60% of the isothermal load needed for failure at the beginning of cooling.

The specimens were placed inside a thermal chamber, equipped with a heater and a liquid nitrogen input to allow for PID-controlled temperature rates.<sup>5</sup> Temperature measurements were taken from two thermocouples placed along the center of the specimen at different distances from the gage section. Digital Image Correlation (DIC) was used for measuring displacements and determining strain fields on the surface of the specimen, which was speckled with thin layers of high-temperature paint before testing. The specimens were first held at zero load and heated to 150 °C, well

<sup>5</sup> The authors would like to acknowledge the help of Kirk, Rohmer, and Wheeler in performing the experiments.

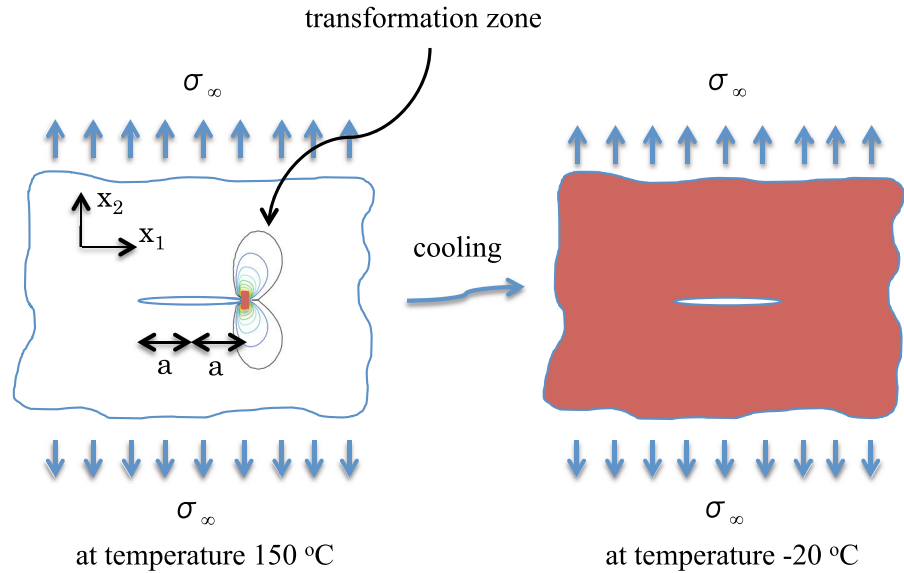
at 60 °C. The phase transition temperatures for this material are  $M_f = -4$  °C,  $M_s = 85$  °C,  $A_s = 21$  °C, and  $A_f = 100$  °C. A video of the evolution of the aforementioned strain component during the experiment can be found here (Supplementary material 2)

above the austenitic-finish temperature, to minimize forward transformation during loading, and then loaded isothermally up to a tensile load level that was equal to a fraction of the experimentally-determined ultimate load at that temperature. Once loaded, the specimens were cooled down at a rate of 10 °C/min while the applied load was held constant to induce forward transformation. Strain field images from these tests (Fig. 18) showed significant strain generation near the notches when the temperature was lowered sufficiently to initiate global martensitic transformation that resulted in catastrophic failure for the cases with sufficient applied load levels.

### 3.2 Numerical simulations

In this section, preliminary results on the effect of thermomechanically-induced phase transformation on the driving force for crack growth and toughness enhancement associated with crack advance are presented in a first attempt to understand SMA response during actuation in the presence of a crack. The prototype infinite center-crack problem is analyzed via the finite element method (Fig. 19). The thermomechanically-

**Fig. 19** Boundary value problem for an infinite center-cracked SMA plate subjected to cooling under constant uniaxial tensile applied load. The region of fully transformed material is represented with the red color



cal loading path used in the analysis is an idealization of typical loading paths that utilize SMAs as actuators subject to constant external mechanical loading under temperature variations. The constitutive model employed in the calculations is developed within the framework of continuum thermodynamics and adopts the classical rate-independent small-strain flow theory for the evolution equations of the transformation strains (Lagoudas et al. 1996; Lagoudas 2008; Lagoudas et al. 2012). The material system Ni<sub>60</sub>Ti<sub>40</sub> (wt%) used in the experiments presented in Sect. 3.1 is chosen, subjected to in-plane uniform uniaxial tensile stress at infinity,  $\sigma_\infty = 250$  MPa, in the direction perpendicular to the crack axis under plane strain conditions. The transformation strain magnitude is a function of the stress state with a saturated value of maximum attainable transformation strain, equal to 0.0135 (Hartl et al. 2011). The mechanical load is applied at 150 °C. At this temperature, the size of the transformation zone is small compared to the crack length  $2a$  and small-scale transformation conditions prevail. Then the temperature is cooled down to  $-20$  °C while the bias load is kept fixed. The temperature distribution is assumed uniform throughout the material at every instant, i.e., latent heat effects are neglected by assuming the rate of both the mechanical and thermal loading being sufficiently slow with respect to the time rate of heat transfer by conduction.

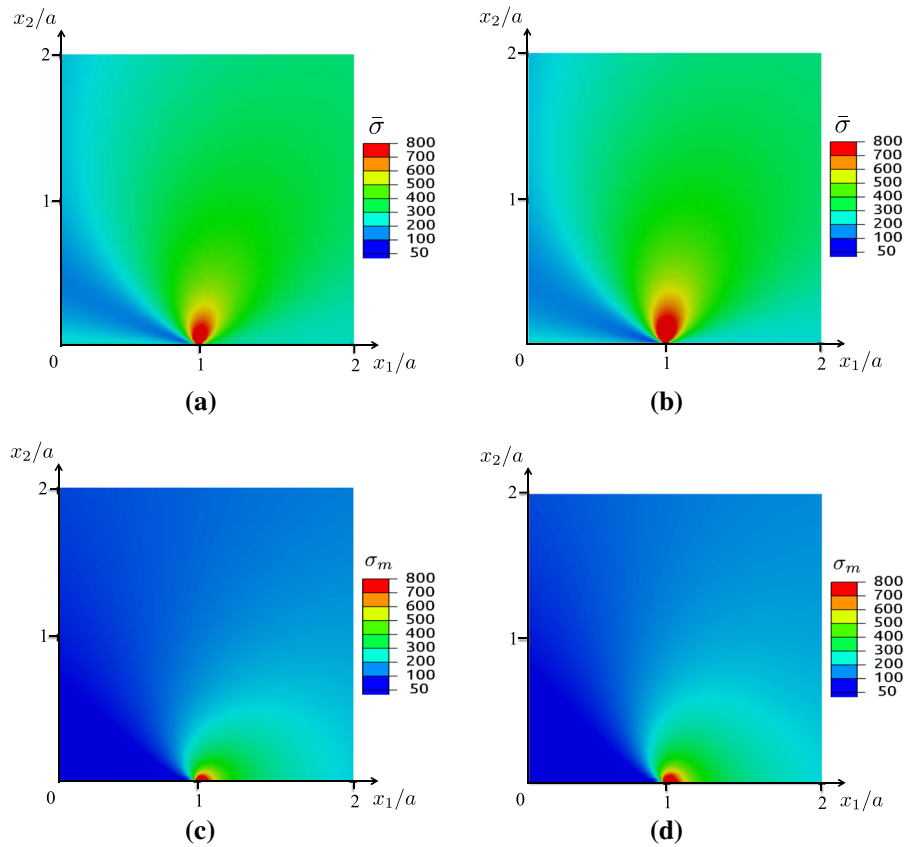
The driving force for crack growth is identified to be the crack-tip energy release rate,  $G_I$ , which is calcu-

lated using the virtual crack closure technique (VCCT) (Rybicki and Kanninen 1977; Krueger 2004; Xie and Biggers 2006). The inherent assumptions in using VCCT are considered acceptable for the constitutive material behavior used in the analysis, which results in a linear elastically-deformed martensite region surrounding the crack tip, and a justification is offered by the calculated crack-tip stress fields in the next section.

### 3.2.1 Static cracks

The thermomechanically-induced phase transformation results in a stress redistribution that changes the crack-tip stress field, as shown in Fig. 20, in which the von Mises stress and mean normal stress,  $\sigma_m = 1/3 \cdot (\sigma_{11} + \sigma_{22} + \sigma_{33})$ , distributions at the crack tip are presented prior to thermal cycling (i.e., at  $T = T_h$ ) and at the end of cooling (i.e., at  $T = T_c$ ). The numerical results suggest that close to the crack tip the stresses always have a  $1/\sqrt{r}$  radial asymptotic behavior. In Fig. 21, the angular dependence of the SMA stress field close to the crack tip at the end of cooling is compared to the angular dependence of the calculated stress field for an isotropic linear elastic solid. According to the calculations, the stress field close to the crack tip for an SMA material is equivalent to that of an isotropic linear elastic material. Therefore, the stress and strain fields close to the crack tip can be characterized by either  $G_I$  or the crack-tip stress intensity factor,  $K_I$ , which is related to  $G_I$  (see Fig. 21) by  $G_I = (1 - \nu^2)K_I^2/E_M$ . This

**Fig. 20** Normalized von Mises stress,  $\bar{\sigma}/\sigma_{\infty}$ , and mean normal stress,  $\sigma_m/\sigma_{\infty}$ , distributions near the crack tip.  $\bar{\sigma} = \sqrt{2/3 \cdot \sigma'_{ij}\sigma'_{ij}}$ , where  $\sigma'_{ij}$  are the components of the deviatoric stress tensor, and  $\sigma_m = 1/3 \cdot (\sigma_{11} + \sigma_{22} + \sigma_{33})$ , where  $\sigma_{ij}$  are the components of the stress tensor. **a** von Mises stress at  $T = T_h$ , prior to cooling. **b** von Mises stress at the end of cooling. **c** Mean normal stress at  $T = T_h$ , prior to cooling. **d** Mean normal stress at the end of cooling



result, apart from justifying the assumption of a single parameter being capable of describing the mechanical fields close to the crack tip, validates the VCCT in calculating that parameter. However, it only holds true for sufficient large sizes of the fully transformed martensitic region close to the crack tip. At higher temperatures close to  $T_h$  and small sizes of the fully transformed martensitic region, which dictate an even smaller size for the region of  $K_I$ -dominance, a discrepancy between the calculated SMA stress field and the mode I elastic asymptotic  $K_I$ -field is observed. It is likely that the stress fields in those cases are evaluated outside the  $K_I$ -dominance region, where higher order terms in the series expansion of the crack-tip stress field are significant (Baxevanis et al. 2014b).

The effect of thermomechanically-induced phase transformation on the driving force for crack growth during cooling under constant applied load, as given by the ratio  $G_I/G_{\infty}$ , is shown in Fig. 22, where  $G_{\infty}$  corresponds to the value of the energy release rate due to the mechanical load alone, prior to cooling, at a temperature sufficiently high so that the material is initially

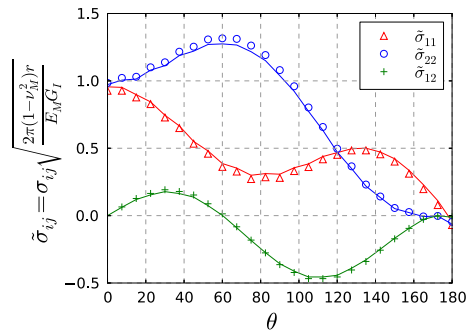


**Fig. 21** Angular distribution of stresses close to the crack tip at the end of cooling. The markers are the numerical results for the SMA material and the solid lines are numerical results for an elastic material with the properties of martensite. The  $1/\sqrt{r}$  radial dependence has been accounted for within the normalization

in the austenitic state (Parrinello et al. 2013; Baxevanis et al. 2015). During cooling the energy release rate increases before attaining a value at temperature  $T = M_f$ , at which point the entire material is fully transformed, which remains constant under cooling at



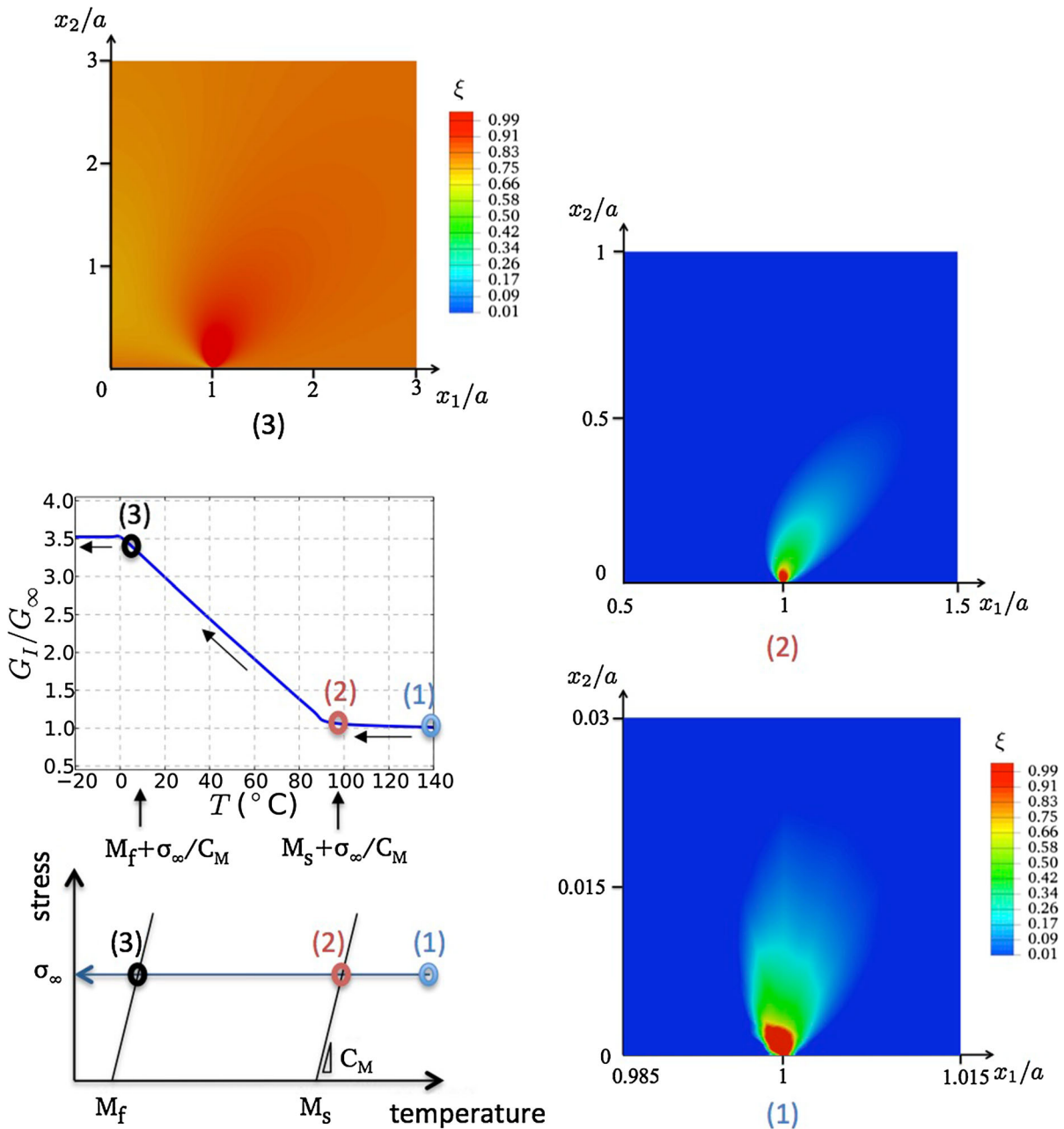


**Fig. 22** Normalized energy release rate,  $G_I/G_\infty$ , versus temperature,  $T$ , during cooling and distribution of martensite volume fraction,  $\xi$ , at different temperatures. At  $T = M_s + \sigma_\infty/C_M$ , the entire material starts transforming into martensite.  $G_\infty$  denotes

the  $G_I$ -value at the end of the mechanical loading step prior to cooling. Note that the regions close to the crack tip in which the contours are plotted are different for visualization purposes

lower temperatures. Thus, if crack growth is assumed to occur when the crack-tip energy release rate reaches a material specific critical value related to the marten-

sitic phase, then crack growth may occur during thermal variations under constant applied loading as a result of phase transformation.

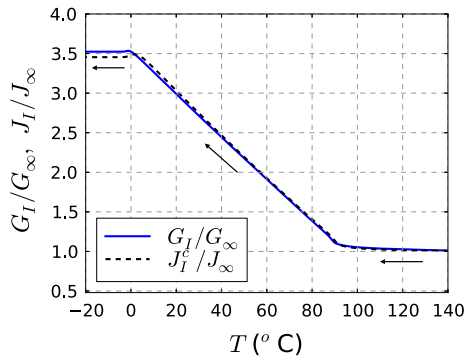


**Fig. 23** Normalized energy release rate,  $G_I/G_\infty$ , and normalized  $J$ -values,  $J_I/J_\infty$ , versus temperature  $T$ .  $J_I^c$  stands for the  $J_I$ -value at the first ring of elements surrounding the crack tip and  $J_I^f$  stands for the  $J_I$ -value at a far-field ring of elements.  $G_\infty$  and  $J_\infty$  denote the respecting values of  $G_I$  and  $J_I$  at the end of the mechanical loading step prior to cooling

Note that (i) the normalized ratio  $G_I/G_\infty$  is independent of the crack length  $2a$ , an expected result since the crack length is the only length scale in the considered fracture problem. (ii) The far-field (at infinity) material starts transforming into martensite during cooling at temperature  $T = M_s + \sigma_\infty/C_M$ , at which the far-field stress,  $\sigma_\infty$ , is equal to the stress required for initiation of phase transformation. At that temperature, which corresponds to global transformation, the increase of the energy release rate is about 8%. (iii) The peak  $G_I/G_\infty$ -value during cooling, which is approximately equal to 3.5, are not attributed just to the elastic moduli mismatch,  $E_M/E_A \approx 0.68$ . Numerical calculations for  $E_A = E_M$  still show a similar substantial enhancement of the energy release rate that should be attributed to stress redistribution caused by large-scale transformation.

The obtained results on the energy release rate are compared against calculations of the  $J$ -integral. Although a strong path-dependency of the  $J$ -integral is observed, similarly to center-cracked panels of conventional elastic-plastic materials loaded in tension under large-scale yielding (Hutchinson 1983), the crack-tip  $J$ -value is very close to the obtained energy release value (Fig. 23). This is another verification of the VCCT employed in the calculations since two different methodologies in computing the same value of driving force for crack growth, i.e., VCCT and the domain integral method, yield close values.

### 3.2.2 Crack growth

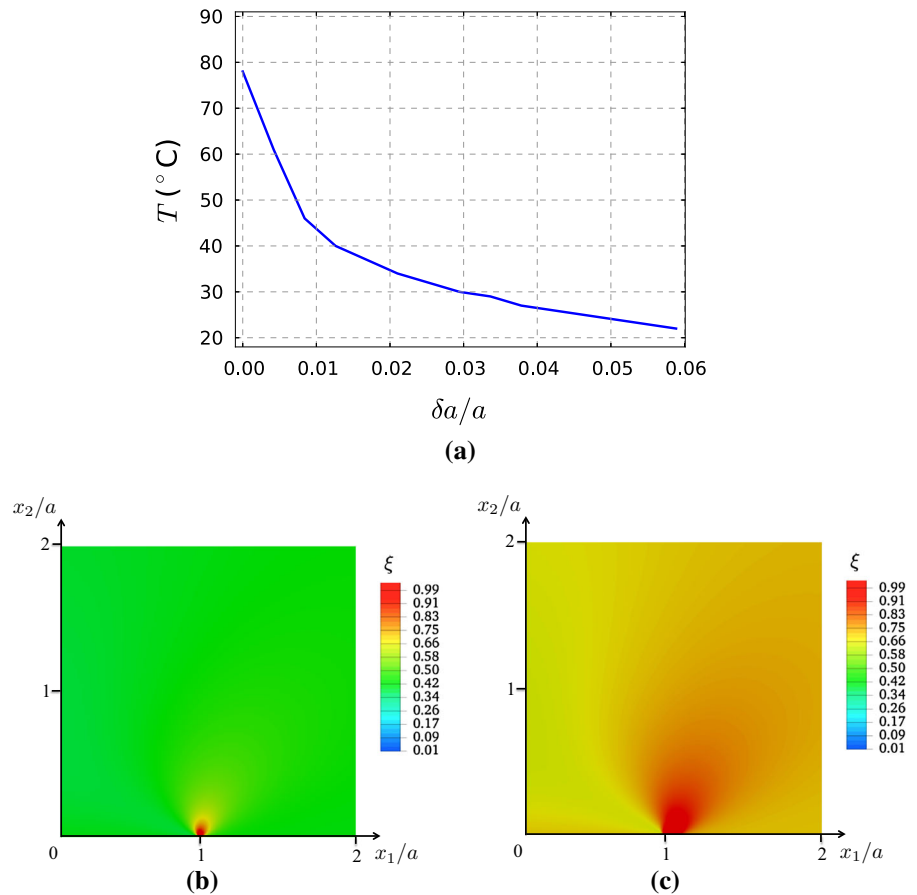
As indicated above, the energy release rate may reach the material specific *critical* value during cooling under a constant mechanical load and initiate crack growth. Results on the possibility of stable crack growth are now presented (Jape et al. 2014, 2015). The material specific critical energy release rate,  $G_{crit}$  is set at a higher value compared to the energy release rate attributed to mechanical loading alone ( $G_{crit} = 2G_\infty$ ), but low enough to be reached during cooling, thereby initiating crack growth. The crack grows stably into a region that is fully transformed into the martensitic state. This transformation toughening response is quite similar to the one due to stress-induced phase transformation in pseudoelastic SMAs in which cracks are observed to grow in an initially stable manner under increasing load (or, depending on the loading arrangement, load-point displacement) until critical conditions are attained resulting in catastrophic failure. As the temperature lowers, the increment of the temperature needed to achieve a given increment of growth is decreasing and eventually instability sets in resulting in catastrophic failure (Fig. 24). The transformation region at initiation of crack propagation and at catastrophic failure are also shown in Fig. 24.

## 4 Discussion

Although considerable progress has been achieved in the assessment of the fracture response of SMAs under mostly applied mechanical load, clearly further experimental and modeling work is needed to fully understand the influence of stress-induced phase transformation, major microstructural factors, and the stress state and loading history on the fracture response of these materials. The fracture mechanics of SMA actuators under combined thermal and mechanical loading is under very early stages of understanding with limited predictive modeling and experimental results. A major challenge is capturing the SMA fracture response under thermomechanical loading paths that involve large-scale phase transformation at the initiation of crack growth and associated strong configurational dependence.

Non-exhaustively, the knowledge acquired so far by the scientific community on the fracture of SMAs includes the following key results:

**Fig. 24** **a** Temperature vs normalized crack growth.  $\delta a$  denotes increments of the crack length  $a$ . **b** Martensite volume fraction distribution near the crack tip at initiation of crack growth; **c** Martensite volume fraction distribution near the crack tip at failure. The spatial variables are normalized by the initial crack length,  $a$ . A video of the crack growth simulation can be found here (Supplementary material 3)



- Stress-induced phase transformation was observed near the crack tip in mechanically loaded single crystal and polycrystalline SMA material systems using in situ synchrotron X-ray diffraction measurements and IR thermographic images.
- Experimental evidence on binary pseudoelastic polycrystalline NiTi shows that plasticity plays a much smaller role than in conventional elastic-plastic materials: (i) cleavage fracture and river markings consistent with markings from traditional brittle intermetallic alloys were reported in NiTi systems containing semi-coherent precipitates; (ii) the crack tips were observed to remain sharp during crack growth; and (iii) all martensitic features in front of the crack tip were found to disappear upon unloading.
- In accordance with the above experimental evidence, finite element analysis showed that martensitic transformation increases the required mechanical load to produce plastic deformation resulting in

plastic zone sizes at the vicinity of the crack tip an order of magnitude smaller than the size expected in conventional elastic-plastic materials.

- Stable crack growth was observed experimentally in single crystal and polycrystalline SMAs, which is primarily associated with the energy dissipated by the stress-induced phase transformed material left behind the advancing crack tip.
- Reverse phase transformation observed due to unloading in the wake of the growing crack and reorientation of martensitic variants distinguish the fracture toughening response of SMAs from that of other dissipative systems. The combined effect of the resulting stress redistribution and energy dissipation associated with reverse phase transformation on the fracture toughness was investigated in finite element simulations of steady crack growth. According to the numerical results, the higher the tendency of the material to reverse transform back to austenite in the wake of the growing

crack, the higher the levels of toughness enhancement.

- By comparing the fracture toughness enhancement obtained in finite element simulations of steady crack growth under isothermal and adiabatic conditions, the generation of latent heat under the adiabatic conditions conditions was shown to reduce the levels of toughness enhancement.
- Experimental evidence suggests that crack growth may occur due to phase transformation resulting from thermal variations under a constant bias load that is considerably lower than the isothermal load needed for crack growth at the beginning of cooling. From an energetic point of view, this SMA fracture response seems to contradict the general view of dissipative processes resulting in toughness enhancement.
- Numerical results indicate that the above characteristic behavior of SMAs should be attributed to stress redistribution induced by large-scale phase transformation.
- Stable crack growth was observed numerically during cooling under constant bias load associated primarily with stress redistribution resulting from the transformed material left behind the growing crack tip.

Future experimental and modeling research studies that may greatly impact the understanding of fracture properties and practice of fracture mechanics concepts in SMAs are discussed below.

- Standards for reliable estimates of the fracture toughness in SMAs are still lacking. Finite element analyses are required to determine  $K$ - and  $J$ -dominance conditions as a function of the ratio of the size of the transformation/detwinning zone over the size of the unbroken ligament in suggested crack configurations in accordance with the ASTM standards. Analytical expressions of the size of the transformation/detwinning zone should be used to confirm whether these conditions are satisfied at the experimentally determined initiation toughness values  $K_c$  or  $J_c$ .
- The microstructural fracture initiation sites and fracture micro-mechanisms should be examined with experiments that shed light on the fracture response in a triaxial stress state. For example, notched cylindrical specimens can be used for this purpose to distinguish, as far as possible, structural effects from intrinsic properties while different notch root radii will allow for different triaxial stress states.
- Stable crack growth and associated toughness enhancement should be examined under actuation loading paths, that involve combined thermal and mechanical loading. Such studies should be performed on a variety of crack configurations and under actuation loading paths beyond that of thermal actuation under constant stress in an effort to reveal the influence of stress triaxiality and fill the gap between the test and working conditions.
- The effect of mechanical and thermal loading rate and the associated latent heat effect on the fracture response should be determined experimentally. Depending on the geometry, convective boundary conditions, and associated heat transfer, the generation or absorption of latent heat may have a strong impact on the deformation response and in turn to the fracture behavior of these materials.
- Fracture experiments should be performed on SMA material systems of the same composition that have been heat treated using different heat-treatment conditions, untrained and trained, in an effort to reveal the influence of precipitation and transformation-induced plasticity (TRIP) on their fracture properties.
- Advancements in the constitutive laws used in the simulations of crack growth are required in order to account for TRIP, reorientation of martensitic variants, transformation anisotropy, minor loops, and thermomechanical coupling at the crack tip. The resulted stress redistribution and/or energy dissipation are expected to have an influence on the fracture response of SMAs that needs to be quantified.
- The successful integration of SMAs into commercial applications beyond the biomedical industry will not only determine the technological importance and the extent of research on the fracture mechanics of SMAs in the near future but is also highly dependent itself on the level of understanding of the fracture properties of these materials. In this regard, there is also a need for studying viscoplastic crack growth in high-temperature SMAs and dynamic fracture.
- Apart from the global approach to fracture, micro-mechanical fracture studies coupled with advances in technologies related to in situ experiments, such as X-ray micro-computed tomography, may offer the opportunity to deepen understanding of the frac-

ture response of SMAs in the future. Such fracture simulations can potentially result in criteria that will connect fracture resistance to measurable and hopefully controllable thermomechanical characteristics and microstructural features to provide a knowledge base that can be used in the design and optimization of SMA material systems and devices.

**Acknowledgments** This material is based upon work supported by the National Science Foundation under Grant Numbers CMMI-1301139 and DMR-0844082.

## References

- Baxevanis T, Chemisky Y, Lagoudas D (2012) Finite element analysis of the plane strain crack-tip mechanical fields in pseudoelastic shape memory alloys. *Smart Mater Struct* 21. doi:[10.1088/0964-1726/21/9/094012](https://doi.org/10.1088/0964-1726/21/9/094012)
- Baxevanis T, Lagoudas D (2012) A mode I fracture analysis of a center-cracked infinite shape memory alloy plate under plane stress. *Int J Fract* 175(2):151–166
- Baxevanis T, Landis C, Lagoudas D (2014a) On the effect of latent heat on the fracture toughness of pseudoelastic shape memory alloys. *J Appl Mech Trans ASME* 81(10). doi:[10.1115/1.4028191](https://doi.org/10.1115/1.4028191)
- Baxevanis T, Landis C, Lagoudas D (2014b) On the fracture toughness of pseudoelastic shape memory alloys. *J Appl Mech Trans ASME* 81(4). doi:[10.1115/1.4025139](https://doi.org/10.1115/1.4025139)
- Baxevanis T, Parrinello A, Lagoudas D (2013) On the fracture toughness enhancement due to stress-induced phase transformation in shape memory alloys. *Int J Plast* 50:158–169
- Baxevanis T, Parrinello A, Lagoudas D (2015) On the driving force for crack growth during thermal actuation of shape memory alloys. Submitted
- Birman V (1998) On mode I fracture of shape memory alloy plates. *Smart Mater Struct* 7:433–437
- Budniansky B, Hutchinson J, Lambropoulos J (1983) Continuum theory of dilatant transformation toughening in ceramics. *Int J Solids Struct* 19:337–355
- Carka D, Landis C (2011) On the path-dependence of the  $J$ -integral near a stationary crack in an elastic-plastic material. *J Appl Mech Trans ASME* 78. doi:[10.1115/1.4001748](https://doi.org/10.1115/1.4001748)
- Creuziger A, Bartol L, Gall K, Crone W (2008) Fracture in single crystal NiTi. *J Mech Phys Solids* 56:2896–2905
- Daymond M, Young ML, Almer J, Dunand D (2007) Strain and texture evolution during mechanical loading of a crack tip in martensitic shape-memory NiTi. *Acta Mater* 55:3929–3942
- Desindes S, Daly S (2010) The small-scale yielding of shape memory alloys under mode III fracture. *Int J Solids Struct* 47:730–737
- Duerig T, Pelton A, Stöckel D (1999) An overview of nitinol medical applications. *Mater Sci Eng A* 273–275, 149–160
- Dugdale D (1960) Yielding of steel sheets containing slits. *J Mech Phys Solids* 8:100–104
- E1820 (2013) Standard test method for measurement of fracture toughness. ASTM International, West Conshohocken
- Freed Y, Banks-Sills L (2007) Crack growth resistance of shape memory alloys by means of a cohesive zone model. *J Mech Phys Solids* 55:2157–2180
- Gall K, Yang N, Sehitoglu H, Chumlyakov Y (2001) Fracture of precipitated NiTi shape memory alloys. *Int J Fract* 109:189–207
- Gollerthan S, Young M, Neuking K, Ramamurty U, Eggeler G (2009a) Direct physical evidence for the back-transformation of stress-induced martensite in the vicinity of cracks in pseudoelastic niti shape memory alloys. *Acta Mater* 57(19):5892–5897
- Gollerthan S, Young ML, Baruj A, Frenzel J, Schmahl W, Eggeler G (2009b) Fracture mechanics and microstructure in NiTi shape memory alloys. *Acta Mater* 57:1015–1025
- Hartl D, Lagoudas D (2007) Aerospace applications of shape memory alloys. In: Proceedings of the institution of mechanical engineers, Part G. *J Aerosp Eng SAGE*, pp 535–552
- Hartl D, Lagoudas D, Calkins F (2011) Advanced methods for the analysis, design, and optimization of sma-based aerostructures. *Smart Mater Struct* 20(9). doi:[10.1088/0964-1726/20/9/094006](https://doi.org/10.1088/0964-1726/20/9/094006)
- Hazar S, Zaki W, Moumni Z, Anlas G (2015) Modeling of steady-state crack growth in shape memory alloys using a stationary method. *Int J Plast* 67:26–38
- He Y, Sun Q (2011) On non-monotonic rate dependence of stress hysteresis of superelastic shape memory alloy bars. *Int J Solids Struct* 48(11–12):1688–1695
- He Y, Yin H, Zhou R, Sun Q (2010) Ambient effect on damping peak of NiTi shape memory alloy. *Mater Lett* 64(13):1483–1486
- Holtz R, Sadananda K, Imam M (1999) Fatigue thresholds of NiTi alloy near the shape memory transition temperature. *Int J Fatigue* 21:S137–S145
- Hutchinson J (1968) Singular behavior at the end of a tensile crack in a hardening material. *J Mech Phys Solids* 16:13–31
- Hutchinson J (1983) Fundamentals of the phenomenological theory of nonlinear fracture mechanics. *J Appl Mech Trans ASME* 50(4B):1042–1051
- Irwin G (1968) Linear fracture mechanics, fracture transition, and fracture control. *Eng Fract Mech* 1(2):241–257
- Jape S, Baxevanis T, Lagoudas D (2014) Stable crack growth during actuation in shape memory alloys, vol 9058. In: Proceedings of SPIE—the international society for optical engineering. doi:[10.1117/12.2048590](https://doi.org/10.1117/12.2048590)
- Jape S, Baxevanis T, Lagoudas D (2015) Actuation-induced toughness enhancement in shape memory alloys. Under preparation
- Krueger R (2004) Virtual crack closure technique: history, approach, and applications. *Appl Mech Rev* 57(2):109–143. doi:[10.1115/1.1595677](https://doi.org/10.1115/1.1595677)
- Lagoudas D (ed) (2008) Shape memory alloys: modelling and engineering applications. Springer, New York
- Lagoudas D, Bo Z, Qidwai M (1996) A unified thermodynamic constitutive model for SMA and finite element analysis of active metal matrix composites. *Mech Compos Mater Struct* 4:153–179
- Lagoudas D, Entchev P, Popov P, Patoor E, Brinson L, Gao X (2006) Shape memory alloys. Part II: modeling of polycrystals. *Mech Mater* 38:430–462

- Lagoudas D, Hartl D, Chemisky Y, Machado L, Popov P (2012) Constitutive model for the numerical analysis of phase transformation in polycrystalline shape memory alloys. *Int J Plast* 32–33:158–183
- Lexcellent C, Laydi MR, Taillebot V (2011a) Analytical prediction of the phase transformation onset zone at a crack tip of a shape memory alloy exhibiting asymmetry between tension and compression. *Int J Fract* 169(1):1–13
- Lexcellent C, Laydi R, Taillebot V (2011b) Impact of the choice of a 3D thermomechanical model for shape memory alloys on the fracture and the delamination predictions. In: *Procedia engineering*, vol 10. pp 2232–2237
- Lexcellent C, Thiebaud F (2008) Determination of the phase transformation zone at a crack tip in a shape memory alloy exhibiting asymmetry between tension and compression. *Scr Mater* 59:321–323
- Loughran G, Shield T, Leo P (2003) Fracture of shape memory CuAlNi single crystals. *Int J Solids Struct* 40(2):271–294
- Machado L (2007) Shape memory alloys for vibration isolation and damping. Ph.D. thesis, Texas A&M University, College Station
- Maletta C (2012) A novel fracture mechanics approach for shape memory alloys with trilinear stress–strain behavior. *Int J Fract* 177(1):39–51
- Maletta C, Furgiele F (2010) Analytical modeling of stress-induced martensitic transformation in the crack tip region of nickel–titanium alloys. *Acta Mater* 58:92–101
- Maletta C, Furgiele F (2011) Fracture control parameters for NiTi based shape memory alloys. *Int J Solids Struct* 48:1658–1664
- Maletta C, Sgambitterra E, Furgiele F (2013) Crack tip stress distribution and stress intensity factor in shape memory alloys. *Fatigue Fract Eng Mater Struct* 36(9):903–912
- Maletta C, Young M (2011) Stress-induced martensite in front of crack tips in NiTi shape memory alloys: modeling versus experiments. *J Mater Eng Perform* 20(4–5):597–604
- McMeeking R, Evans A (1982) Mechanics of transformation-toughening in brittle materials. *J Am Ceram Soc* 65:242–246
- Miyazaki S (1990) *Engineering aspects of shape memory alloys*. Butterworth-Heinemann, London
- Miyazaki S, Imai T, Igo Y, Otsuka K (1986) Effect of cyclic deformation on the pseudoelastic characteristics of Ti–Ni alloys. *Metall Trans A* 17A(1):115–120
- Nespoli A, Besseghini S, Pittaccio S, Villa E, Viscuso S (2010) The high potential of shape memory alloys in developing miniature mechanical devices: a review on shape memory alloy mini-actuators. *Sens Actuator A Phys* 158(1):149–160
- Otsuka K, Wayman C (eds) (1999) *Shape memory materials*. Cambridge University Press, Cambridge
- Parrinello A, Baxevanis T, Lagoudas D (2013) On the energy release rate during global thermo-mechanically-induced phase transformation in shape memory alloys, vol. 2 of ASME 2013 conference on smart materials, adaptive structures and intelligent systems, SMASIS 2013. doi:10.1115/SMASIS2013-3187
- Patooor E, Lagoudas D, Entchev PB, Brinson L, Gao X (2006) Shape memory alloys. Part I: general properties and modeling of single crystals. *Mech Mater* 38:391–429
- Pelton A, DiCello J, Miyazaki S (2000) Optimisation of processing and properties of medical grade nitinol wire. *Minim Invas Ther Allied Technol* 9(2):107–118
- Petrini L, Migliavacca F (2011) Biomedical applications of shape memory alloys. *J Metall*. doi:10.1155/2011/501483
- Prahlad H, Chopra I (2003) Development of a strain-rate dependent model for uniaxial loading of SMA wires. *J Intell Mater Syst Struct* 14(14):429–442
- Rice J (1967) Stresses due to a sharp notch in a work-hardening elastic-plastic material loaded by longitudinal shear. *ASME J Appl Mech* 34:287–298
- Rice J (1968) A path independent integral and approximate analysis of strain concentration by notches and cracks. *ASME J Appl Mech* 35:379–386
- Rice J, Rosengren G (1968) Plane strain deformation near a crack tip in a power-law hardening material. *J Mech Phys Solids* 16:1–12
- Robertson S, Mehta A, Pelton A, Ritchie R (2007a) Evolution of crack-tip transformation zones in superelastic Nitinol subjected to in situ fatigue: a fracture mechanics and synchrotron X-ray microdiffraction analysis. *Acta Mater* 55(18):6198–6207
- Robertson S, Metha A, Pelton A, Ritchie R (2007b) Evolution of crack-tip transformation zones in superelastic Nitinol subjected to in situ fatigue: a fracture mechanics and synchrotron X-ray micro-diffraction analysis. *Acta Mater* 55:6198–6207
- Robertson S, Pelton A, Ritchie R (2012) Mechanical fatigue and fracture of nitinol. *Int Mater Rev* 57(1):1–36
- Robertson S, Ritchie R (2007) In vitro fatigue–crack growth and fracture toughness behavior of thin-walled superelastic nitinol tube for endovascular stents: a basis for defining the effect of crack-like defects. *Biomaterials* 28(4):700–709
- Robertson S, Ritchie R (2008) A fracture-mechanics-based approach to fracture control in biomedical devices manufactured from superelastic nitinol tube. *J Biomed Mater Res B* 84(1):26–33
- Rybicki E, Kanninen M (1977) A finite element calculation of stress intensity factors by a modified crack closure integral. *Eng Fract Mech* 9:931–938
- Shaw J, Kyriakides S (1995) A phenomenological model for pseudoelasticity of shape memory alloys under multiaxial proportional and nonproportional loadings. *J Mech Phys Solids* 43(1):1243–1281
- Sree Kumar M, Nagarajan T, Singaperumal M, Zoppi M, Molfino R (2007) Critical review of current trends in shape memory alloy actuators for intelligent robots. *Ind Robot* 34(4):285–294
- Stam G, van der Giessen E (1995) Effect of reversible phase transformations on crack growth. *Mech Mater* 21:51–71
- Stoeckel D, Pelton A, Duerig T (2004) Self-expanding nitinol stents: material and design considerations. *Eur Radiol* 14(2):292–301
- Vaidyanathan R, Dunand D, Ramamurty U (2000) Fatigue crack-growth in shape-memory NiTi and NiTi–TiC composites. *Mater Sci Engi A* 289(1–2):208–216
- Vasko G, Leo P, Shield T (2002) Prediction and observation of crack tip microstructure in shape memory CuAlNi single crystals. *J Mech Phys Solids* 50(9):1843–1867

- Wang G (2007a) Effect of martensite transformation on fracture behavior of shape memory alloy NiTi in a notched specimen. *Int J Fract* 146:93–104
- Wang G (2007b) A finite element analysis of evolution of stress–strain and martensite transformation in front of a notch in shape memory alloy NiTi. *Mater Sci Eng A* 460–461
- Wang X, Wang Y, Baruj A, Eggeler G, Yue Z (2005) On the formation of martensite in front of cracks in pseudoelastic shape memory alloys. *Mater Sci Eng A* 394:393–398
- Xie D, Biggers S (2006) Progressive crack growth analysis using interface element based on the virtual crack closure technique. *Finite Elem Anal Des* 42:977–984
- Xiong F, Liu Y (2007) Effect of stress-induced martensitic transformation on the crack tip stress-intensity factor in Ni–Mn–Ga shape memory alloy. *Acta Mater* 55:5621–5629
- Yan W, Mai Y (2006) Theoretical consideration on the fracture of shape memory alloys, vol 127. Springer, Netherlands
- Yan Y, Yin H, Sun Q, Huo Y (2012) Rate dependence of temperature fields and energy dissipations in non-static pseudoelasticity. *Contin Mech Thermodyn* 24(4–6):675–695
- Yi S, Gao S (2000) Fracture toughening mechanism of shape memory alloys due to martensite transformation. *Int J Solids Struct* 37:5315–5327
- Yi S, Gao S, Shen S (2001) Fracture toughening mechanism of shape memory alloys under mixed-mode loading due to martensite transformation. *Int J Solids Struct* 38:4463–4476
- Yin H, Yan Y, Huo Y, Sun Q (2013) Rate dependent damping of single crystal CuAlNi shape memory alloy. *Mater Lett* 109:287–290
- Yoon S, Yeo D (2008) Experimental investigation of thermo-mechanical behaviors in Ni–Ti shape memory alloy. *J Intell Mater Syst Struct* 19(3):283–289
- Young M, Gollerthan S, Baruj A, Frenzel J, Schmahl W, Eggeler G (2013) Strain mapping of crack extension in pseudoelastic niti shape memory alloys during static loading. *Acta Mater* 61(15):5800–5806